Contribution from the Department of Chemistry,
William Marsh Rice University, Houston, Texas 77001

Spectroscopic Study of a Series of Iron Carbido Clusters

B. A. SOSINSKY,* N. NOREM, and J. SHELLY

Received January 6, 1981

The ^{57}Fe Mössbauer and ESCA spectra of $[Fe_6C(CO)_{16}]^{2-}$, $[Fe_5C(CO)_{15}]$, $[Fe_5C(CO)_{14}]^{2-}$, $[Fe_4C(CO)_{12}]^{2-}$, $[Fe_4C(CO)_{12}H]^-$, $[Fe_4(CH)(CO)_{12}H]$, $[Fe_4(\mu\text{-}CO)(CO)_{12}H]^-$, and θ-Fe_3C have been measured. Direct observation of cluster carbido ESCA carbon $1s_{1/2}$ peaks at 287.7-293.0 eV suggests a relatively deshielded carbon atom with a general trend toward nucleophilic character as the carbon coordination number is reduced. A concomitant trend toward enhanced cluster carbonyl bonding is observed. An explanation of trends based on a molecular orbital scheme is advanced. The relevance of these observations to the possible nature of active surface carbon on iron as implied by these compounds is discussed.

Introduction

The series (Figure 1) of iron carbonyl carbido clusters $[Fe_6C(CO)_{16}]^{2-}$ (Fe_6^{2-}), $[Fe_5C(CO)_{14}]^{2-}$ (Fe_5^{2-}), $[Fe_5C(CO)_{15}]$ (Fe_5^0), $[Fe_4C(CO)_{12}]^{2-}$ (Fe_4^{2-}), $[Fe_4C(CO)_{12}H]^-$ (Fe_4^-), $[Fe_4C(CO)_{13}]$ (Fe_4^0), a related methyne cluster $[Fe_4(CH)(CO)_{12}H]$ ($Fe_4(CH)^0$), a dinuclear iron carbene cluster $[Fe_2(CH_2)(CO)_8]$ ($Fe_2(CH_2)^0$), a bent carbonyl cluster $[Fe_4(\mu\text{-}CO)(CO)_{12}H]^-$ ($Fe_4(\mu\text{-}CO)^-$), and the heterogeneous iron carbide cementite, θ-Fe_3C, form the basis of our spectroscopic study. The compounds were studied with use of ESCA, photoelectron-induced Auger electron, solution infrared, and Mössbauer spectroscopy, techniques that provide *quantitative measure of the charge on the constituent atoms as a function of electron-cloud shielding parameters*. The objectives of the study were to obtain an understanding of the charge distribution in the polyhedral array and, in particular, the direct characterization of the carbido carbon atom in the various clusters so that comparisons of these species with surface states may be made. Measurements of Mössbauer isomer shifts and iron $2p_{3/2}$ ESCA peaks provide direct quantification of the average charge on polyhedral iron and are presented. The carbon $1s_{1/2}$ ESCA peaks described present a quantification of the average charge on carbonyl and *carbido* carbon atoms, giving a measure of the degree of cluster-carbonyl π back-bonding in the former case and presenting direct unambiguous spectroscopic characterization of the nature of carbido carbon in the latter. Oxygen ESCA $1s_{1/2}$ peaks are an additional measure of cluster-carbonyl π back-bonding, which have been correlated with the multiplicity weighted average $\langle\nu_{CO}\rangle$. We present two-dimensional plots of incident X-ray energy corrected strong-line Auger peaks vs. ESCA photoelectron peaks for iron and oxygen, which further substantiate bonding patterns and trends among the series of compounds studied. We also present a bonding scheme that rationalizes the variation in the observed spectroscopic parameters.

The possible relevance of the spectra of these compounds to carbon formed from carbon monoxide adsorbed on iron and its reactivity is discussed. Modern spectroscopic tools such as ESCA,[1-7] AES,[8] LEED,[6,7] and SIMS,[9] which characterize the surface state of chemisorbed species, have been applied to the iron catalysts so that there currently exists a body of data delineating the static nature of the active iron metal surfaces. In addition, several methods have been utilized to define the internal state of the bulk of small iron crystallites such as Mössbauer spectroscopy,[10-16] magnetic susceptibility,[17-20] and X-ray diffraction[17,21,22] and these serve as a further comparison. Although these clusters do not appear to be active working models,[23] the spectroscopic parameters are consistent with observed surface states[2] and structural comparison may be made on this basis.

Experimental Section

All complexes were synthesized and handled under rigorous air-free conditions with use of standard techniques.[24] The following compounds were synthesized by literature methods: $(Et_4N)^+_2[Fe_6C(CO)_{16}]^{2-}$,[25] $(Et_4N)^+_2[Fe_5C(CO)_{14}]^{2-}$,[26] $[Fe_5C(CO)_{15}]$,[27,28] $(PPN)^+_2[Fe_4C(CO)_{12}]^{2-}$,[29] $(Et_4N)^+[Fe_4C(CO)_{12}H]^-$,[29] $[Fe_4(CH)(CO)_{12}H]$,[30] $(C_5H_5N)^+[Fe_4(\mu\text{-}CO)(CO)_{12}H]^-$.[31,32] Cementite ($Fe_3C$)

(1) Rhodin, T. H.; Ertl, G. "The Nature of the Surface Chemical Bond"; North-Holland Publishing Co.: Amsterdam, 1979.
(2) Plummer, E. W.; Salaneck, W. R.; Miller, J. S. *Phys. Rev. B: Condens. Matter* **1978**, *18*, 1673.
(3) Brodén, G.; Gafner, G.; Bonzel, H. P. *Appl. Phys.* **1977**, *13*, 333.
(4) Brodén, G.; Gafner, G.; Bonzel, H. P. *Surf. Sci.* **1979**, *84*, 295.
(5) Atkinson, S. J.; Brundle, C. R.; Robert, M. W. *J. Electron Spectrosc. Relat. Phenom.* **1973**, *2*, 105.
(6) Brundle, C. R. *IBM J. Res. Dev.* **1978**, *22*, 235.
(7) Textor, M.; Gay, I. D.; Mason, R. *Proc. R. Soc. London, Ser. A* **1977**, *356*, 37.
(8) Dwyer, D. J.; Somorjai, G. A. *J. Catal.* **1978**, *52*, 291.
(9) Oh, G. L.; Fleisch, T.; Delgass, W. N. *J. Catal.* **1979**, *58*, 394.
(10) Dumesic, J. A. *Adv. Catal.* **1977**, *26*, 121. See ref 75.
(11) Amelese, J. A.; Butt, J. B.; Schwartz, L. H. *J. Phys. Chem.* **1978**, *82*, 558.
(12) Raupp, G. B.; Delgass, W. N. *J. Catal.* **1979**, *58*, 337.
(13) Raupp, G. B.; Delgass, W. N. *J. Catal.* **1979**, *58*, 348.
(14) Raupp, G. B.; Delgass, W. N. *J. Catal.* **1979**, *58*, 361.
(15) Schäfer-Stahl, H. *Angew. Chem., Int. Ed. Engl.* **1980**, *19*, 729.
(16) Delgass, W. N., personal communication.
(17) Storch, H.; Golumbic, N.; Anderson, R. B. "The Fischer-Tropsch and Related Syntheses"; Wiley: New York, 1951.
(18) Loktev, S. M.; Makarenkova, L. I.; Slivinskii, E. V.; Entin, S. D. *Kinet. Catal.* **1972**, *13* (2), 933.
(19) Pichler, H.; Kruger, E. *Brenst.-Chem.* **1966**, *47*, 368.
(20) von Wolf, W.; Copeman, J. *Brenst.-Chem.* **1965**, *46*, 149.
(21) Hägg, G. *Z. Kristallogr., Kristallgeochem., Kristallphys., Kristallchem.* **1934**, *89*, 92.
(22) Eckstrom, H. C.; Adcock, W. A. *J. Am. Chem. Soc.* **1950**, *72*, 1042.
(23) Muetterties, E. L.; Stein, J. *Chem. Rev.* **1979**, *79*, 479 and references contained therein.
(24) Shriver, D. F. "The Manipulation of Air Sensitive Compounds"; McGraw-Hill: New York, 1969.
(25) Stewart, R. P.; Ander, U.; Graham, W. A. G. *J. Organomet. Chem.* **1971**, *32*, C49.
(26) Cooke, C. G.; Mays, M. J. *J. Organomet. Chem.* **1975**, *88*, 231.
(27) Tachikawa, M.; Muetterties, E. L. *J. Am. Chem. Soc.* **1980**, *102*, 4541.
(28) Braye, E. H.; Dahl, L. F.; Hubel, W.; Wampler, D. L. *J. Am. Chem. Soc.* **1962**, *84*, 4633.
(29) $(Et_4N)^+_2[Fe_6C(CO)_{16}]^{2-}$ was stirred in dry THF with tropylium fluoroborate for 24 h. The solution was evaporated and the residue extracted with hexane. The remaining residue was recrystallized from THF/ether/hexane. The infrared and mass spectra were matched to those in ref 52. We note that an intermediate species is initiating hydrogen abstraction from THF.
(30) $(Et_4N)^+[Fe_4C(CO)_{12}H]^-$ was stirred for 12 h in trifluoroacetic acid. The solution was then evaporated, and the residue was recrystallized from hexane. The infrared and mass spectra were matched to those in ref 27.
(31) Hieber, W.; Werner, R. *Chem. Ber.* **1975**, *90*, 286.
(32) Manassero, M.; Sansoni, M.; Longoni, G. *J. Chem. Soc., Chem. Commun.* **1976**, 919.

0020-1669/82/1321-0348$01.25/0

Table I. ^{57}Fe Mössbauer Spectra

compd	$\delta^{a,b}$	Δ^{a}	fwhm^{a,c}	form^{f}	ref
$(Et_4N)^+_2[Fe_6C(CO)_{16}]^{2-}$	0.417		2.55	273 K, SP	
$(Et_4N)^+_2[Fe_5C(CO)_{14}]^{2-}$	0.354		1.80	273 K, SGM	
$[Fe_5C(CO)_{15}]$	0.200	0.460	2.10	273 K, SGM	
$(PPN)^+_2[Fe_4C(CO)_{12}]^{2-}$	0.237	0.671	0.95	273 K, SGM	
$(Et_4N)^+[Fe_4C(CO)_{12}H]^-$	0.183	0.955	1.55	80 K, SP	
$[Fe_4(CH)(CO)_{12}H]$	0.354		3.85	80 K, SGM	
$(C_5H_5N)^+[Fe_4(\mu\text{-}CO)(CO)_{12}H]^-$	0.33	0.67	0.44	80 K, SGM	35
Fe_3C	0.29	*g*		80 K, SP	75
$[Fe(CO)_5]$	0.17	2.57	0.26	80 K, FS	35
$[Fe_2(CO)_9]$	0.42	0.42	0.36	80 K, SP, SGM	35
$[Fe_3(CO)_{12}]$	0.37, 0.31	1.13, 0.13	0.30, 0.28	80 K, SP	35
$Na_2[Fe(CO)_4]^{2-}$	0.08	0.18	0.35	80 K, NS	35
$(Et_4N)^+_2[Fe_2(CO)_8]^{2-}$	0.18	2.22	0.31	80 K, NS	35
$[Fe(en)_3]^{2+}[Fe_3(CO)_{11}]^{2-}$ *d,e*	0.16	2.11	0.35	80 K, NS	35
$(Et_4N)^+_2[Fe_4(CO)_{13}]^{2-}$	0.28	0.27	0.33	80 K, NS	35
$(Et_4N)^+[Fe(CO)_4H]^-$	0.09	1.36	0.30	80 K, NS	35
$(Et_4N)^+[Fe_2(CO)_8H]^-$	0.33	0.50	0.31	80 K, NS	35
$(Et_4N)^+[Fe_3(CO)_{11}H]^-$	0.30, 0.28	1.41, 0.16	0.28, 0.30	80 K, FS	35

[a] In mm/s. [b] Relative to iron metal foil. [c] Full line width at half-maximum height. [d] en = ethylenediamine. [e] Anion only; cation has δ = 1.38 mm/s, Δ = 1.19 mm/s. [f] SGM = silicon grease mull, SP = solid pellet, FS = frozen solution. [g] H = 208 kOe. Both types of iron have fields degenerate within ±5 kOe.

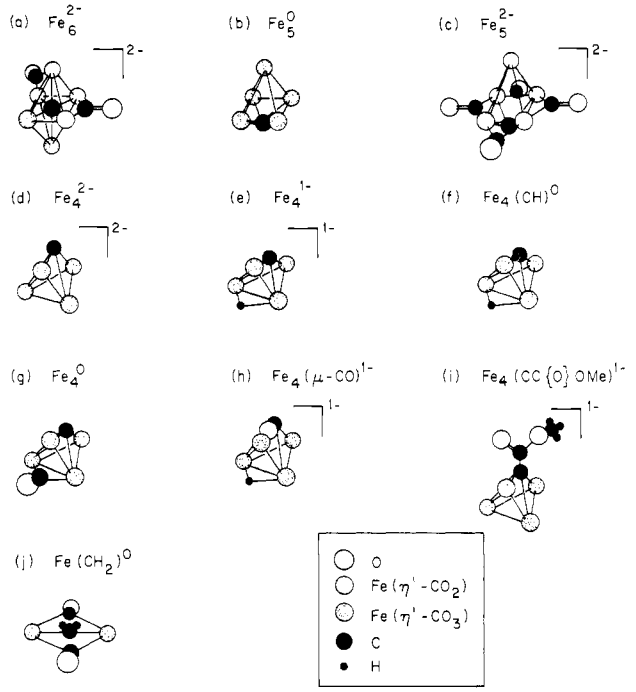

Figure 1. Metal carbonyl cluster complexes: (a) $(Et_4N)_2[Fe_6C(CO)_{16}]^{2-}$ (Fe_6^{2-}); (b) $[Fe_5C(CO)_{15}]$ (Fe_5^0); (c) $(Et_4N)^+_2[Fe_5C(CO)_{14}]^{2-}$ (Fe_5^{2-}); (d) $(PPN)^+_2[Fe_4C(CO)_{12}]^{2-}$ (Fe_4^{2-}); (e) $(Et_4N)^+[Fe_4C(CO)_{12}H]^-$ (Fe_4^-); (f) $[Fe_4(CH)(CO)_{12}H]$ ($Fe_4(CH)^0$); (g) $[Fe_4C(CO)_{13}]$ (Fe_4^0); (h) $(C_5H_5N)^+[Fe_4(\mu\text{-}CO)(CO)_{12}H]^-$ ($Fe_4(\mu\text{-}CO)^-$); (i) $(Et_4N)^+\{Fe_4[CC(O)OMe](CO)_{12}\}^-$ ($\{Fe_4[CC(O)OMe]\}^-$); (j) $[Fe_2(CH_2)(CO)_8]$ ($Fe_2(CH_2)^0$).

was obtained from commercial sources[33] and characterized by elemental analysis and X-ray powder diffraction. Two compounds, $[Fe_4C(CO)_{13}]$ and $[Fe_2(CH_2)(CO)_8]$, were obtained from others and sublimed prior to use.

The iron-57 Mössbauer spectra were run either in the solid state or as a silicone grease mull in the form indicated and as described elsewhere.[34] Sample sizes were 0.2–0.4 g of iron compounds, and collection time was 1–2 days. Spectra were taken at room temperature and liquid nitrogen temperature, and the sharpest spectra were used in this study.

X-ray photoelectron spectra were obtained with use of a Varian IEE ESCA spectrometer with an aluminum (Al Kα) anode source operating at 10 KV and 100 mA giving incident X-ray energy of 1486.6 eV. Scanning was done in 0.1–0.5 eV steps by varying a retarding voltage applied to the sample. A constant pass energy of 100 eV was used, giving a constant 1-eV instrumental line width. The carbon spectra were obtained with use of software that eliminated the Al $K\alpha_{3,4}$ satellite, to provide optimum carbon data. Samples (0.2 g) were carefully ground in a glovebox and dusted onto double-sided Scotch (polymer) tape and mounted into the machine in the exclusion of air. Care was taken to completely cover the tape to eliminate extraneous carbon or oxygen signals. The samples $(Et_4N)^+[Fe_4C(CO)_{12}H]^-$ and $(C_5H_5N)^+[Fe_4(\mu\text{-}CO)(CO)_{12}H]^-$ were not ground prior to measurement of their photoelectron spectra due to the sensitivity of surface nitrogen atoms to X-ray radiation. Two compounds, $[Fe_4C(CO)_{13}]$ and $[Fe_2(CH)_2(CO)_8]$, decomposed rapidly under the X-ray flux, and XPS spectra were not obtainable, but we did not observe decomposition of the other compounds in the times measured. We measured regions normally associated with the following electron emissions: Fe $2p_{1/2}$ and $2p_{3/2}$ (710–740 eV), C $1s_{1/2}$ (296–266 eV), O $1s_{1/2}$ (524–544 eV), Fe L_3VV Auger line (764–814 eV), C KLL Auger line (1210–1260 eV), O KVV Auger line (960–1010 eV), N $1s_{1/2}$ (390–410 eV).

The true binding energy of all photolines was assumed to be (observed photolines) − 0.3 eV. This correction was determined with use of the observed Et_4N^+ nitrogen photolines in two cases by comparison to Et_4NCl and by comparison to the oxidized iron samples' iron $2p_{3/2}$ peak with reported values for iron oxide. We estimate the error in the binding energies to be of the order ±0.3 eV. This charge-referencing procedure generates spectra for which the observed photolines are in accord with those measured previously in the Varian spectrometer. We note solid-state photoline values are several eV smaller than gas-phase values.[2]

Results and Discussion

^{57}Fe Mössbauer Spectroscopy. The ^{57}Fe Mössbauer spectra of the compounds studied are listed in Table I along with a series of related compounds measured by other workers.[35] Mössbauer spectroscopy measures the effect of incident γ rays upon the nuclear levels of the Mössbauer-active isotope. A chemical shift in the form of an isomer shift (δ) is measured relative to a standard in a velocity adjusted by Doppler-shifting the source. Isomer shifts are most sensitive to electron-cloud screening and are commonly interpreted in the form of oxidation state or charge on the observed atom. All the carbido complexes measured were found to be broad singlets or poorly resolved doublets that the computer program could not further resolve. Therefore, no effects due to asymmetry about the iron atoms as measured by a quadrupole splitting (Δ) could be

(33) Cerac/Pure Division, Box 1178, Milwaukee, Wis. 53201.
(34) Tweedle, M. F.; Wilson, L. J. *J. Am. Chem. Soc.* **1976**, *98*, 4824.
(35) Famery, K.; Kilner, M.; Greatrex, W.; Greenwood, N. N. *J. Chem. Soc. A* **1969**, 2339.

measured. Broadness in the Mössbauer spectrum can be attributed[36,37] to several causes, the most obvious being the presence of several different iron atoms. Lack of a rigid lattice leading to recoil also leads to line broadening. Indeed, we had difficulty measuring useful spectra on several of our compounds in their crystalline form and had to resort to measuring their spectra in the form of silicone grease mulls,[35] which sharpened the spectra considerably.

Several trends have been noted[35] in the observed isomer shifts for the binary iron carbonyl series. The isomer shift is reduced (enhanced nuclear screening) as anionic charge on the cluster increases, as exemplified by the series $[Fe_2(CO)_9] > [Fe_2(CO)_8H]^- > [Fe_2(CO)_8]^{2-}$. Also, as the coordination number at iron increases, the isomer shift increases (reduced nuclear screening). Replacement of a bridging carbonyl group by a hydride ligand increases the quadrupole splitting and reduces the isomer shift.

Most interestingly, we observe trends distinctly different for the carbido cluster series than was observed for the simpler binary iron carbonyls. The complex Fe_5^0 had a somewhat lower isomer shift than the other complexes measured, lower, in fact, than Fe_5^{2-}. Accumulation of negative charge in the Fe_5^0 cluster framework leads to enhanced screening decreasing the average δ value at iron. This suggests that the iron framework is somewhat more electron rich in Fe_5^0 than in the Fe_5^{2-} carbido cluster. These two clusters are presumed to be isostructural, with Fe_5^0 and Fe_5^{2-} both 84-electron clusters.[38,39] In the dianion the additional electron density is formally metal–ligand in nature. The decreased isomer shift for Fe_5^0 suggests that electron charge residing in the iron framework is shifted to the carbido carbon atom in Fe_5^{2-}. A distortion of the framework toward octahedral may be occurring for Fe_5^{2-}. The distortion would be of the type observed for Fe_4^{2-} vs. $Fe_4(CO)^0$ (both are 60-electron clusters) where the dianion distorts to accommodate an additional two framework electrons by a decrease in the dihedral angle about carbon and a lengthening of the iron to carbon bonds.[40] We expect to observe a similar deshielding of Fe_4^{2-} relative to Fe_4^0.

Another trend we sought to establish was the variation of isomer shift for a series as a function of carbon atom coordination number as provided by the series Fe_6^{2-}, Fe_5^{2-}, and Fe_4^{2-}. As the carbon atom becomes more exposed, a progressive decrease in the isomer shift occurs, signifying an enhanced average degree of screening at iron in going from Fe_6^{2-} to Fe_4^{2-}. Accumulation of excess negative charge per iron atom would establish the decreasing trend. Nucleophilic behavior may be involved in the formation of $\{Fe_4[CC(O)OMe](CO)_{12}H\}^-\{Fe_4[CC(O)OMe]\}^-$ from the oxidative degradation of Fe_6^{2-} by tropylium ion in methanol.[41] If there is a tendency for the carbido carbon atom to become more nucleophilic with decreasing coordination number and with increased charge per iron atom, then this trend should lead to a decrease in the amount of the expected drop in isomer shifts for the series $Fe_6^{2-} > Fe_5^{2-} >> Fe_4^{2-}$, which we see for Fe_5^{2-} vs. Fe_4^{2-}. As the average iron coordination number decreases (Fe_6^{2-}–Fe_4^{2-}), an increase in isomer shift is also expected. With two trends operating in opposite directions,[35] it is difficult to make a substantiative conclusion regarding the change in carbon atom character in this series by Mössbauer spectroscopy. ESCA data presented later makes more substantiative conclusions. The complication of variation in cluster-carbonyl bond strength, discussed later, must also be considered.

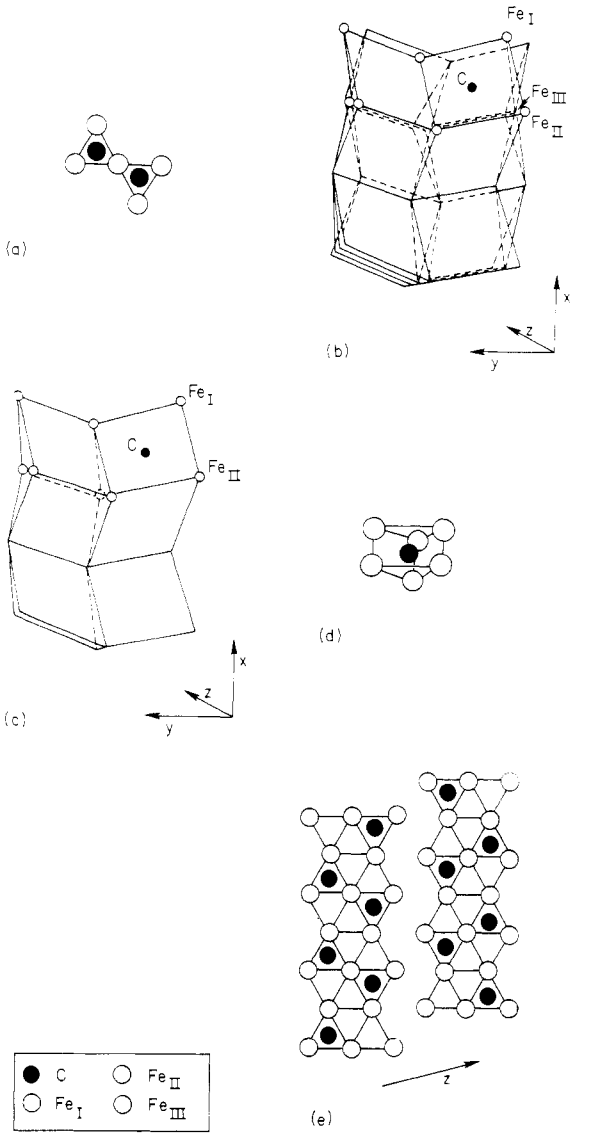

Figure 2. Heterogeneous iron carbides: (a) top view of χ-Fe_5C_2; (b) multi-unit-cell packing of Hägg carbide, χ-Fe_5C_2; (c) multi-unit-cell packing of cementite, θ-Fe_3C; (d) unit cell of θ-Fe_3C; (e) two-monolayer packing of χ-Fe_5C_2, xy plane. Iron directions indicate magnetic equivalences.

The Fe_4 butterfly clusters illustrate the effect of proton addition to the cluster framework. As Fe_4^{2-} is first monoprotonated and then diprotonated to give first Fe_4^- and then $Fe_4(CH)^0$, the spectra broaden and the isomer shift decreases, consistent with previous observations. The mechanism by which a cluster hydride reduces the isomer shift is a matter of conjecture, but suggestions[35] have ranged from the hydride ion involvement in iron to hydrogen σ d-electron donation or the alternate explanation that hydride as a strong σ donor increases the electric field at the nucleus. We attribute the spectral broadening in the Fe_4 series to increased asymmetry in the cluster that could not be resolved.

Mössbauer spectroscopy has been used to study the carbiding of iron catalysts and serves as a surface technique especially for small iron crystallites.[10] Several different types of iron carbides have been characterized under iron-catalyzed CO hydrogenation reaction conditions with use of Mössbauer spectroscopy.[12-15] The procedure involves computer-fitting of

(36) Greenwood, N. N.; Gibb, T. C. "Mössbauer Spectroscopy"; Chapman and Hall: London, 1971.
(37) Drago, R. S. "Physical Methods in Chemistry"; W. B. Saunders Company: Philadelphia, 1977.
(38) Wade, K. "Electron Deficient Compounds"; Appleton-Century-Crofts, New York, 1971.
(39) Wade, K. *Adv. Inorg. Chem. Radiochem.* **1976**, *18*, 1.
(40) Bradley, J. S. Southwest Catalysis Society Meeting, Nov 1980, Rice University, Houston, Texas.
(41) Bradley, J. S.; Ansell, G. B.; Hill, E. W. *J. Am. Chem. Soc.* **1979**, *101*, 7417.

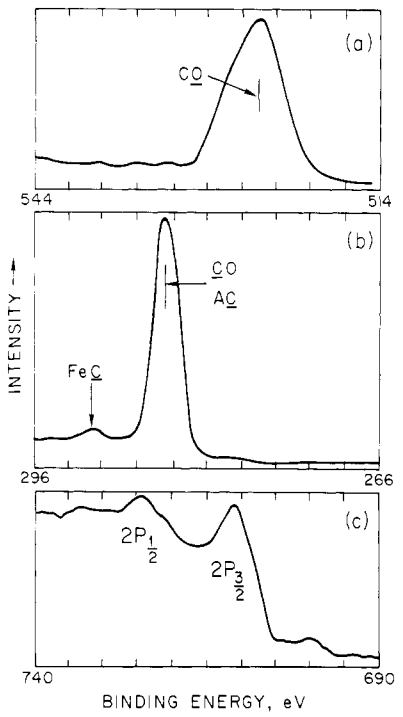

Figure 3. ESCA spectrum of $(PPN)^+_2[Fe_4C(CO)_{12}]^{2-}$: (a) oxygen $1s_{1/2}$ region, 544–514 eV (carbonyl oxygen = *CO*); (b) carbon $1s_{1/2}$ region, 296–266 eV (carbonyl carbon = *C*O; carbido carbon = Fe*C*; aryl carbon = A*C*); (c) iron $2p_{1/2}$ and $2p_{3/2}$ region, 740–690 eV.

the spectrum using the experimental isomer shift and hyperfine field splitting, which, along with an experimentally observed Curie temperature, serves as a comparison with known, structurally characterized iron carbides. The particle size of the crystallites studied is sufficiently small (100-Å range) so that Mössbauer reveals the environment of a large fraction of surface iron. It is also possible to size the particles using Mössbauer spectroscopy.[10] Four binary iron carbides (see Figure 2) have been identified: ϵ'-$Fe_{2.2}C$ (hexagonal close-packed, $T_c \approx 720$ K), ϵ-$Fe_{2.2}C$ (transition from hexagonal close-packed to monoclinic, $T_c = 650$ K), χ-Fe_5C_2 (Hägg structure–monoclinic, $T_c = 525$ K), and θ-Fe_3C (cementite–orthorhombic, $T_c = 480$ K).[12] The ϵ' and ϵ phases can be identified, forming first in the catalyst. These two phases appear preferentially hydrogenable.[16] As the catalyst ages, the bulk is carbided with the χ phase and the ϵ' phase disappears.[12] The χ phase forms because of the reaction conditions. Higher temperatures favor the formation of θ-Fe_3C. Furthermore, it was found that the extent of carbiding tracks the increase in catalytic activity and that higher hydrocarbons become favored as the iron carbides.[14] Hydrogenation of bulk iron carbide was found to be very slow after a certain amount of surface carbide is hydrogenated and selective for methane formation.[14] Recent work has questioned the appearance of the ϵ phase.[15,16]

ESCA Data. The X-ray photoelectron spectra of the compounds under study are tabulated in Table II. XPS or ESCA[42-48] is a relatively nondestructive spectroscopic technique in which core electrons are ejected by an incident X-ray beam. The energy of the free electron is characteristic of a particular element and core level but is influenced by the valence shell of the atom, giving rise to chemical state data commonly interpreted in the form of an oxidation state but more correctly interpreted in terms of an atomic charge in the form of a binding energy. Oxidation states are an arbitrary parameter, but the charge of an atom may be directly calculated and measured and is a property of bonding and local electron field density. An atom in a given oxidation state in similar compounds can exhibit a wide range of atomic charges. ESCA is a surface technique that can register constituents of a surface to the depth of 5–40 Å, which, in the case of our complexes, represents a depth of 2–3 monolayers. The comparison[2] of heterogeneous and homogeneous systems requires careful charge referencing and solid-state data.[46-48,76]

The most sensitive iron photoline is the $2p_{3/2}$ level, and the range found for reduced iron in the clusters studied was 707.9–710.5 eV; cementite, Fe_3C, was measured at 707.2 eV. This range is well within a range found for other formally low-valent iron carbonyls (e.g., $Fe(CO)_5$ at 709.1–709.7 eV). Cementite falls in the range normally associated[44] with iron metal (707–708 eV), indicating its metallic-covalent nature.

The series Fe_6^{2-}, Fe_5^{2-}, and Fe_4^{2-} illustrates an isoelectronic series in which the major distinction is the drop in carbon atom coordination number. The series had peaks measured at 708.2, 707.9, and 710.5 eV, respectively, showing that the iron environment first becomes more shielded (greater valence electron density) and then becomes less shielded. Increased valence electron density increases shielding in the sense that core levels are shielded from nuclear charge, leading to lower core level binding energies. Transfer of valence electron density to carbon from iron as carbon coordination number decreases would establish a rising trend in the binding energy for iron. The Fe_5^{2-} cluster is therefore, by this reasoning, more shielded at iron than Fe_6^{2-}. A binding energy rise at iron in Fe_4^{2-} is, therefore, due to increased charge transfer to a nucleophilic carbon atom.

Comparison of the Fe_5^0 and Fe_5^{2-} clusters (709.6 and 707.9 eV) shows that iron is more shielded in the dianion. This was the logical expectation since the dianion has two additional framework electrons concentrated about the iron atoms.[36,37] The Mössbauer isomer shifts showed Fe_5^0 to be more screened at iron than Fe_5^{2-} in contrast to the ESCA data. The Fe_5^0 iron atoms must be more effectively screened at the nucleus to γ radiation than Fe_5^{2-}, whereas the shielding at Fe_5^0 core electron levels is less than that for Fe_5^{2-}. The cause for this discrepancy is most often explained in terms of unusual extranuclear relaxation energies[45] or the fact that Mössbauer spectroscopy is more sensitive to electron density at the nucleus whereas ESCA screening involves all valence levels. For a similar series as shown by the two-dimensional chemical plots (Figures 4 and 5), extranuclear relaxation energies are similar. For broad singlets we feel hesitant in placing more confidence in the Mössbauer δ than in the ESCA data.

The effect of protonation in the series Fe_4^{2-}, Fe_4^-, and $Fe_4(CH)^0$ (710.5, 708.9, and 709.2 eV) illustrates that the framework is sensitive to two different effects. Monoprotonation of the framework (Fe_4^-) draws framework electron density into a metal cluster hydride bond. The second protonation occurs at a carbon–iron bonding edge changing the nature of the metal carbide. The observed rise in binding energy from Fe_4^- to $Fe_4(CH)^0$ illustrates that cluster-coordinated methyne is deshielding at iron relative to carbido

(42) Czanderna, A. W. *Methods Phenom.: Their Appl. Sci. Technol.* **1975**, *1*.
(43) Siegbahn, K.; et al. "ESCA; Atomic Molecular and Solid State Structure Studied by Means of Electron Spectroscopy"; Almquist and Wiksells: Stockholm, 1967.
(44) Siegbahn, K.; et al. "ESCA Applied to Free Molecules"; North-Holland Publishing Co.: Amsterdam, 1969.
(45) Jolly, W. L. *Top. Curr. Chem.* **1977**, *71*, 149–182.
(46) Wagner, C. D. *Anal. Chem.* **1972**, *44*, 967.
(47) Wagner, C. D.; Gale, L. H.; Raymond, R. H. *Anal. Chem.* **1979**, *51*, 466.
(48) Wagner, C. D.; Zatko, D. A.; Raymond, R. H. *Anal. Chem.* **1980**, *52*, 1445.
(49) Kosolapova, T. Ya. "Carbides, Properties, Production and Applications"; Plenum Press: New York, 1971.

Table II. ESCA Data

compd	element	line	cor[a,b] binding energy	assigt[c]	fwhm[a,d]	area[e]
$(Et_4N)^+_2[Fe_6C(CO)_{16}]^{2-}$	Fe	$2p_{1/2}$	723.4			
		$2p_{3/2}$	708.2	Fe	2.5	6.0
		L_3VV	786.4			
	C	$1s_{1/2}$	289.6; 287, 284.6	FeC; CO, CH	~0.5, 2.7	~1, 22.3
		KLL	1227.7			
	O	$1s_{1/2}$	537.5; 532.4	shake-off; CO	~1.6, 2.1	0.2, 4.0
		KVV	978.7			
$(Et_4N)^+_2[Fe_5C(CO)_{14}]^{2-}$	Fe	$2p_{1/2}$	720.4			
		$2p_{3/2}$	711.2; 707.9	FeO; Fe^0	~2.5, 2.5	2.1, 5.0
		L_3VV	786.2			
	C	$1s_{1/2}$	288.8; 285.0	FeC; CO, CH	~1.8, 2.7	2.5, 73.7
		KLL	1277.7			
	O	$1s_{1/2}$	527.9; 532.0	shake-off; CO	~2.5, 3.0	1.93, 22.3
		KVV	975.7			
$[Fe_5C(CO)_{15}]$	Fe	$2p_{1/2}$	722.7			
		$2p_{3/2}$	709.6	Fe^0	2.3	5.0
		L_3VV	786.7			
	C	$1s_{1/2}$	287.7; 284.6	FeC, CO	~1.0, 1.8	0.9, 9.4
		KLL	1227.7			
	O	$1s_{1/2}$	532.1	CO	1.8	5.4
		KVV	979.4			
$(PPN)^+_2[Fe_4C(CO)_{12}]^{2-}$	Fe	$2p_{3/2}$	724.2			
		$2p_{1/2}$	710.5	Fe^0	8.5	4.0
		L_3VV	785.2			
	C	$1s_{1/2}$	290.3; 284.3	FeC; CH, CO	3.0, 2.4	4.3, 10.9
		KLL	1227.7			
	O	$1s_{1/2}$	530.7	CO	5.4	38.8
		KVV	975.7			
$(Et_4N)^+[Fe_4C(CO)_{12}H]^-$	Fe	$2p_{1/2}$	725.1; 721.5			
		$2p_{3/2}$	711.5; 708.9	FeO; Fe^0	~1, ~3.5	3.4, 4.0
		L_3VV	787.5			
	C	$1s_{1/2}$	293.0; 285.4	FeC; CO, CH	3.5, 5.5	0.7, 14.9
		KLL	1227.2			
	O	$1s_{1/2}$	539.4; 533.0	shake-off; CO	3.0, 2.8	0.5, 4.7
		KVV	977.0			
	N	$1s_{1/2}$	402.1	Et_4N	3.8	0.4
$[Fe_4(CH)(CO)_{12}H]$	Fe	$2p_{1/2}$	722.0			
		$2p_{3/2}$	709.2	Fe^0	3.0	4.0
		L_3VV	787.7			
	C	$1s_{1/2}$	284.6	CO, CH	1.8	8.5
		KLL	1228.7			
	O	$1s_{1/2}$	532.3	CO	1.8	0.6
		KVV	979.2			
$(C_5H_5N)^+[Fe_4(\mu\text{-CO})(CO)_{12}H]^-$	Fe	$2p_{1/2}$	723.7; 721.2			
		$2p_{3/2}$	710.9; 708.2	FeO; Fe^0	..., 4.5	sh, 4.0
		L_3VV	786.2			
	C	$1s_{1/2}$	284.7	CO, CH	3.0	6.6
		KLL	1227.2			
	O	$1s_{1/2}$	538.7; 532.0	shake-off; CO	2.0, 3.2	0.7, 10.6
		KVV	976.6			
	N	$1s_{1/2}$	399.6		2.6	0.9
Fe_3C	Fe	$2s_{1/2}$	724.2			
		$2s_{3/2}$	711.2; 707.2	FeO; Fe^0	5.0, ~1.5	10.9, 3.0
		L_3VV	783.1			
	C	$1s_{1/2}$	288.3; 284.7	FeC_s; Cg or FeC_b	~1.0, 2.4	3.6, 68.9
		KLL	1227.2			
	O	$1s_{1/2}$	530.2	FeO	3.4	8.6
		KVV	not measd			

[a] In eV. [b] (Observed binding energies) − 0.3 eV. [c] Abbreviations: FeO = oxidized iron; Fe^0 = reduced iron; FeC = carbido carbon (subscript s = surface, b = bulk); Cg = graphidic carbon; CO = metal carbonyl, CH = organic carbon, shake-off = shake-off peak (π CO orbital). [d] fwhm = full line width at half-maximum height. [e] Elemental sensitivities: Fe $2p_{3/2}$:C $1s_{1/2}$:O $1s_{1/2}$:N $1s_{1/2}$ = 10.5:1.00:2.85:1.78.

carbon in this series, which correlates with the trend of C → CH → CH_2 toward more nucleophilicity.

Oxidized iron was observed in four cases: Fe_5^{2-} (711.2 eV), Fe^0 (711.5 eV), $Fe_4(\mu\text{-CO})^-$ (710.9 eV), and Fe_3C (711.2 eV). We note that after the samples were left overnight in the spectrometer in air, all of the samples' reduced iron (Fe^0) signals were converted to oxidized iron (FeO) that was found to be in the region normally associated with Fe_2O_3. These peaks were coincident in the five cases mentioned above, so we reject the argument that these peaks were different types of reduced iron in the cluster. In the case of $Fe_4(\mu\text{-CO})^-$, an oxidized iron peak was found to be rather low for Fe_2O_3 and may alternately be associated with the iron atom bonded to the multicenter oxygen atom of the bridging μ-CO ligand.[28] We note that in $Fe_4(\mu\text{-CO})^-$ this may be the only case in which two different cluster iron atom core levels may be uniquely differentiated. In other cases the difference between iron atomic charges is sufficiently small so that differences lead only to line broadening.

The carbon $1s_{1/2}$ signal presented us with the best opportunity to observe directly the polyhedral carbon atoms. Ionic metallic carbides (e.g., HgC, ZrC, TiC, NbC, TaC, VC, and WC) are found in the region of 280–283 eV, the more metallic covalent carbides occurring at higher values, a trend estab-

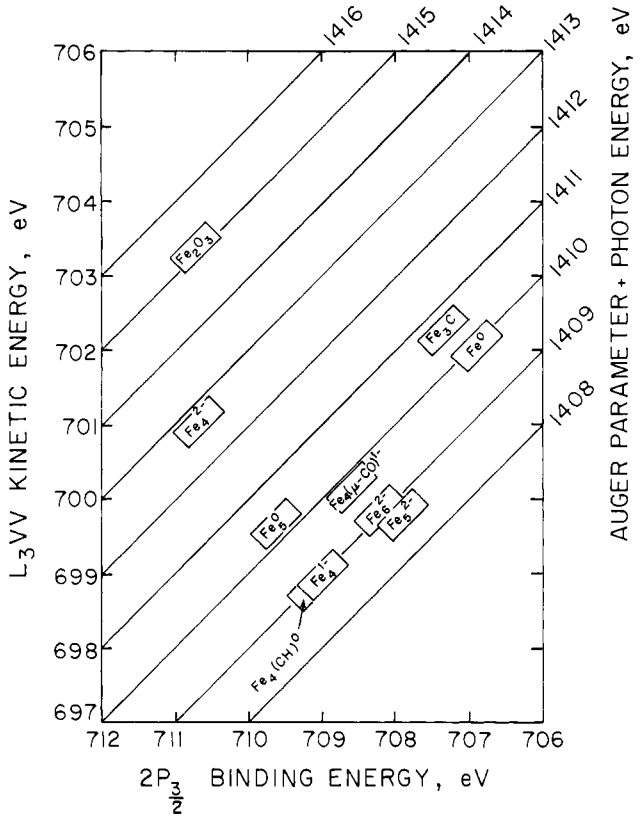

Figure 4. Chemical state plot for the iron L_3VV Auger line vs. $2p_{3/2}$ photoline.

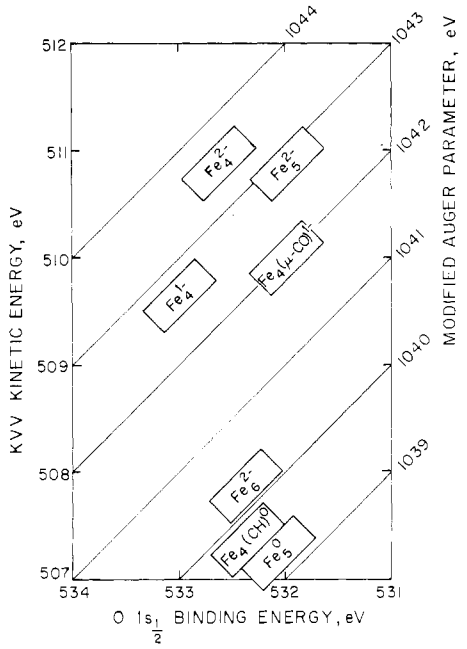

Figure 5. Chemical state plot for the oxygen KVV Auger line vs. $1s_{1/2}$ photoline.

lished rising in a triad and going to the right in the transition series. We measured two carbon signals for cementite at 288.3 and 284.7 eV. The latter signal is within the range of graphitic carbon (284–285 eV) and is either bulk carbide or a graphitic overlayer formed at the surface of the iron/carbon melt or from the decomposition of carbon-containing gases from which cementite is manufactured.[50,51] The more oxidized peak in the C $1s_{1/2}$ region at 288.3 eV we assign to low-coordinate surface iron carbide carbon or near-surface (up to 40 Å deep) carbide. A lesser probability would be surface carbon monoxide. We noted an asymmetric oxygen $1s_{1/2}$ signal that could contain both types of oxygen (bound at carbon and iron) at 530.2 eV and that integrates well against carbon (3.40:1.00) but is in the region more normally associated with Fe_2O_3 (529.7–530.4 eV). We base our assignment for low-coordinate surface carbon, or near-surface carbon, in cementite on similar values found for cluster carbido carbon.

The clusters studied showed two types of carbon $1s_{1/2}$ signals in the regions 287.7–293.0 and 284.3–285.4 eV. Counterions complicated the picture somewhat. We assigned the most oxidized carbon $1s_{1/2}$ signals for Fe_6^{2-} (289.6 eV), Fe_5^{2-} (288.8 eV), Fe_5^0 (287.7 eV), and Fe_4^{2-} (290.3 eV) to carbido carbon atoms. The remaining signals are assigned to carbonyl carbon atoms and alkyl and aryl counterion carbon atoms. In the case of Fe_5^0 absence of a counterion conclusively exhibits carbonyl in the assigned region. In reduced clusters the carbonyl carbon should be shielded relative to $Fe(CO)_5$ and fall in the range of organic carbon as has been found on iron surfaces[4] mentioned later. We note that for the series Fe_6^{2-}, Fe_5^{2-}, and Fe_4^{2-}, the carbido carbon $1s_{1/2}$ signal first drops and then rises in value, mirroring the behavior found in the iron $2p_{3/2}$ signals of this series. The key observation here is the position of carbido carbon in a region substantially deshielded from graphite and bulk iron carbide. Alternate assignments of these peaks to shake-up or shake-off phenomena are unjustified due to the diamagnetic nature of the complexes. Although intense shake-up is a feature of gas-phase C $1s_{1/2}$ XPS spectra (Mg Kα irradiation), our solid-state spectra do not exhibit these features. Another alternative explanation of the oxidized carbon peak as carbonyl does not fit in with integrated intensities of signals, which are more in line with our assignments. The ESCA spectrum of $(PPN)^+_2[Fe_4C(CO)_{12}]^{2-}$ is shown in Figure 3. Most importantly, in cases not containing a carbido carbon atom such as $Fe_4(CH)^0$ and $Fe_4(\mu\text{-}CO)^-$, we fail to detect this more oxidized carbon that we associate with carbido carbon.

Oxygen $1s_{1/2}$ signals assigned to iron carbonyl oxygen atoms were found in the range of 530.7–533.0 eV and are a measure of cluster-carbonyl bonding with decreasing oxygen $1s_{1/2}$ values, arguing for enhanced $Fe_{d\pi} \rightarrow C_{p\pi}$ π back-bonding (Fe═C═O vs. M⁻—C≡O⁺). For the series Fe_6^{2-} (532.4 eV), Fe_5^{2-} (532.0 eV), and Fe_4^{2-} (530.7 eV), we saw a steady trend toward enhanced shielding at oxygen as more charge is concentrated on fewer iron atoms due possibly to a low-coordinate nucleophilic carbon atom, indicating enhanced $Fe_{d\pi} \rightarrow C_{p\pi}$ π back-bonding. This effect is discussed in relation to the cluster molecular orbital picture later on. The effect of going from Fe_5^0 (532.0 eV) to Fe_5^{2-} (532.1 eV) was scarcely noticeable. The four-atom butterfly system O $1s_{1/2}$ was found at Fe_4^{2-} (530.7 eV), Fe_4^- (533.0 eV), and Fe_4^0 (532.3 eV). This indicates monoprotonation of the framework deshields carbonyl oxygen, suggesting less iron–carbon π back-bonding due to the formation of a cluster hydride and removal of polyhedral iron electron density. The second protonation to form methyne shows it to be shielding at oxygen relative to carbido carbon, indicating stronger iron to carbon back-bonding in $Fe_4(CH)^0$ relative to Fe_4^-. The carbido carbon in Fe_4^- withdraws electron density from the cluster framework that methyne does not, again consistent with a low-coordinate nucleophilic carbido carbon atom becoming a more nucleophilic methyne.

We note a feature in the oxygen $1s_{1/2}$ region found for Fe_6^{2-} (537.5 eV), Fe_5^{2-} (537.9 eV), Fe_4^- (530.4 eV), and $Fe_4(\mu\text{-}CO)^-$ (538.7 eV) that is well outside the range normally associated

(50) Toth, L. E. "Transition Metal Carbides and Nitrides"; Academic Press: New York, 1971.

(51) Benziger, J.; Madix, R. J. *Surf. Sci.* **1980**, *94*, 119.

with oxygen.[42] No additional peaks in the $Fe_4(\mu\text{-CO})^-$ O $1s_{1/2}$ region could be found assignable to the unique multicenter carbonyl oxygen. Broad peaks to higher binding energies are normally associated with the shake-off phenomenon where a valence electron is ejected just prior to core electron emission. We note that a high-lying filled metal carbonyl π-orbital electron is mainly centered near the electronegative oxygen atom and would be most likely ejected by scanning the oxygen $1s_{1/2}$ photoelectron range.

The ESCA spectrum of carbon monoxide chemisorbed on α-Fe(100) and polycrystalline iron surfaces has been reported by other workers.[6,7,51] Four distinct chemical states were identified: I (Fe(100), Fe polycrystalline; 293 °C) C $1s_{1/2}$ 282.6 eV and O $1s_{1/2}$ 530.2 eV; II (Fe(100); 293 °C) C $1s_{1/2}$ 284.6 eV and O $1s_{1/2}$ 531.1 eV; III (Fe polycrystalline; 123 °C) C $1s_{1/2}$ 285.6 eV and O $1s_{1/2}$ 532.1 eV; IV (Fe 100, Fe polycrystalline; 123 °C) C $1s_{1/2}$ 285.6 eV and O $1s_{1/2}$ 532.1 eV. States II–IV are suggested to be molecular in nature and state I to be dissociative. We note that in states II–IV the C $1s_{1/2}$ and O $1s_{1/2}$ binding energy values are nearly identical with the assignments made for metal carbonyl ligand carbon and oxygen values in our clusters. ESCA is a matrix-sensitive technique, and these clusters run in the solid state are a similar matrix. This suggests that cluster-ligated carbon monoxide is nearly identical in chemical state to chemisorbed carbon monoxide. The observation that impurity carbon C $1s_{1/2}$ and oxygen O $1s_{1/2}$ peaks present during cleaning and preparation of α-Fe(100) and Fe polycrystalline samples occur at binding values identical with enhanced signals found after carbon monoxide chemisorption led to its assignment as a dissociated state.[6] Iron metal in ordered and disordered crystalline forms has the ability to dissociate carbon monoxide with great facility.[1] The binding energy value found for state I O $1s_{1/2}$ is identical with the value found for O $1s_{1/2}$ measured in our cementite sample, thus confirming our assignment of this peak to low-coordinate iron oxide (FeO_x, $x < 1.5$).

We do not find a peak in any of our ESCA C $1s_{1/2}$ regions that can be assigned to surface carbon reported in state I. All our assignments to carbido carbon C $1s_{1/2}$ peaks are found at 287.7–290.7 eV above the carbonyl monoxide and graphite range in stark contrast to the carbon $1s_{1/2}$ peak in state I, which was measured at 282.6 eV. Admission of hydrogen in the form of hydrogen ion sputtering does not remove this state I carbon peak, and the presence of this peak may be due to a subsurface superlattice ordering effect.[52,53]

Carbido carbon is substantially deshielded relative to inactive surface carbon. If active surface carbon follows the pattern of the cluster compounds, its facile hydrogenation may arise from hydrogen's ability to polarize available electron density toward carbon, an electron-poor center on an electron-rich metal. We note that changes in matrix would tend to shift all photolines in the same direction and the correlation[2] of carbon monoxide values strongly suggests quaternary carbon correlation. The similarity of encapsulated Fe_6^{2-} carbido carbon to exposed carbon atoms suggests that carbon atoms on an iron surface may be relatively mobile and hydrogenable, and such a pattern is suggested[12-15] by the carbiding pattern of small iron crystallites. A near-surface carbide superlattice[52,53] controlled-hydrogenation mechanism[54] presents a rationale for CO bond cleavage that would explain why the rate of carbide formation for iron follows the rate of hydrocarbon synthesis for small iron crystallites.[14,55] The carbide mechanism[56-59] has been supported by isotopic labeling studies on cobalt metal[58,59] as has the function of methylene as the chain growth species.[59] We note that the kinetics[60] of methanation reactions on group 8 metals may be fit to a mechanism of near-surface carbide hydrogenation since movement of hydrogen adsorbed dissociatively through bulk iron is extremely rapid.[61] Group 8 metals perform the Fischer–Tropsch reaction converting synthesis gas (H_2/CO mixtures) to organic compounds.[23,62-71] The SASOL process[72] currently on stream in South Africa employs potassium-fused iron.

For many elements the rather restricted range of core level binding energies limits the amount of information available from ESCA. It has been found that use of the photoelectron-derived strong-line Auger electron signal corrected for the incident X-ray (Al Kα) energy and plotted vs. the binding energy of the most intense photoelectron line for many elements is a useful format for separating compounds into various oxidation states and bonding patterns.[46-48] The Auger parameter is a measure of the extranuclear relaxation energy as higher lying electron levels collapse to fill the core hole. The Auger electron is emitted subsequent to this process. When core Auger levels are used, many compounds are well dispersed and the array can be understood qualitatively in terms of electronegativity of bonding atoms and polarizability of the medium. Valence type Auger lines are less well characterized but are often well dispersed and useful for identification. The iron L_3VV level and oxygen KVV levels are valence type. We have plotted the compounds studied for iron[47] (Figure 4) and oxygen[48] (Figure 5) on two-dimensional chemical state plots. The two-dimensional carbon plots have been found to be too inconsistent to be useful due to a very broad and hard to measure KLL carbon Auger electron spectrum.

The iron two-dimensional chemical state plot, Figure 4, separates the compounds studied into several groups. Cementite falls into an identical region with iron metal on the two-dimensional iron plot, emphasizing the similar metallic nature of iron in this compound. The clusters $Fe_4(\mu\text{-CO})^-$, Fe_5^{2-}, Fe_6^{2-}, Fe_4^-, and $Fe_4(CH)^0$ are all nearly coincident, illustrating the similarity of iron in these cases. The Fe_5^0 cluster is somewhat different but close to this group. In contrast, Fe_4^{2-} is well separated and the iron polyhedral core appears to have a substantially different, possibly smaller, relaxation energy. Relaxation energy has been found to be cordination number dependent, higher valency leading to increased avenues for electron flow.[45] Our observation of the carbido C $1s_{1/2}$ ESCA peak does not indicate it is substantially

(52) Darken, L. S.; Gursy, R. W.; Beaver, M. B. "Physical Chemistry of Metals"; McGraw-Hill: New York, 1953.
(53) Barrett, C. S. "Structure of Metals" McGraw-Hill: New York, 1952.
(54) Sosinsky, B. A., manuscript in preparation.
(55) A reviewer has pointed out that the specific activity of small iron crystallites is an order of magnitude smaller than the actual catalysts. See: Storm and M. Boudart, Proceedings of the North American Catalysis Society Meeting, Chicago, March 1979. See also: Vannice, Proceedings of the VII International Congress on Catalysis, Tokyo, July 1980. The effect of particle size on mechanism to our mind is not understood, but could argue against an interstitial hydrogenation mechanism.
(56) Fischer, F.; Tropsch, H. *Brennst.-Chem.* **1926**, *7*, 97.
(57) Fischer, F.; Tropsch, H. *Chem. Ber.* **1926**, *59*, 830.
(58) Biloen, P.; Helle, J. N.; Sachtler, W. M. H. *J. Catal.* **1926**, *58*, 95.
(59) Brady, R. C., III; Pettit, R. *J. Am. Chem. Soc.* **1981**, *103*, 1287.
(60) Vannice, M. A. *J. Catal.* **1975**, *37*, 449–473.
(61) McLellan, R. *Acta Metall.* **1979**, *27*, 1655.
(62) Pichler, H. *Adv. Catal.* **1952**, *4*, 271.
(63) Masters, C. *Adv. Organomet. Chem.* **1979**, *17*, 61.
(64) King, D. L. *J. Catal.* **1978**, *51*, 386.
(65) Pichler, H.; Schultz, H. *Chem.-Ing.-Tech.* **1970**, *42*, 1162.
(66) Nefedov, B. K.; Eidus, Y. T. *Russ. Chem. Rev.* (*Engl. Transl.*) **1965**, *34*, 272.
(67) Chang, C. D.; Lang, W. H.; Silvestri, A. J. *J. Catal.* **1978**, *56*, 268.
(68) Elvins, O. C.; Nash, A. W. *Nature* (*London*) **1926**, *118*, 154.
(69) Kummer, J. F.; Emmett, P. *J. Am. Chem. Soc.* **1953**, *75*, 5177.
(70) Pichler, H.; Schultz, H. *Chem.-Ing.-Tech.* **1970**, *42*, 1160.
(71) Henrici-Olivé, G.; Olivé, S. *Angew. Chem., Int. Ed. Engl.* **1967**, *15*, 136.
(72) Dry, M. E. *Ind. Eng. Chem. Prod. Res. Dev.* **1976**, *15*, 282.

shielded in the Fe_4^{2-} case. The variation of relaxation energy with coordination number is often responsible for shifting observed photolines and could explain anomalies in expected trends for carbido carbon binding energy values.

The two-dimensional chemical state oxygen plot modified Auger parameter α' vs. O $1s_{1/2}$ binding energy (Figure 5), more indicative of cluster-carbonyl bonding, delineates a distinct separation of the cluster complex carbonyl groups that gives a better measure of the differences and similarities in cluster-carbonyl bonding. Buildup of electron charge on carbonyl oxygen argues for enhanced metal–carbon π back-bonding and decreased valency at oxygen. The separation of cluster-carbonyl oxygen on the chemical state plot is highly significant. One group, Fe_6^{2-}, $Fe_4(CH)^0$, and Fe_5^0, is in a very similar location. The Fe_5^0 carbide cluster is nearly identical with Fe_6^{2-}, which is isostructural with ϵ'-$Fe_{2.2}C$ hexagonal close-packed bulk carbide. Clusters with more exposed carbides, Fe_5^{2-}, Fe_4^-, and Fe_4^{2-}, show a distinct rise in the modified Auger parameters (α'). The values for α' may rise in this series as the number of avenues for relaxation (enhanced π back-bonding) increases due to an increased molecular electron density flow component. The cluster $Fe_4(\mu\text{-CO})^-$ shows decreased cluster-carbonyl bonding intermediate between these two groups.

Chemical state plots of α or α' vs. photoelectron core lines are useful in differentiating bonding groups in a class of compounds but have as yet no obvious predetermined predictive power when valence Auger lines are used, as can be seen by the anomalous dispersion of a variety of iron- and oxygen-containing species.[47,49] Electronic relaxation energy shifts photoelectron lines and is a primary stumbling block to using chemical shifts to study chemical bonding. Approaches to the estimation of relaxation energy treat core ionization as a two-part problem, one term associated with contraction of the local atomic charge distribution and the second term a measure of the relaxation energy associated with the rest of the molecule as electron density flows in to fill the core hole.[45,76]

We sought a correlation between the O $1s_{1/2}$ binding energy for our series of cluster carbido carbonyls and the multiplicity weighted average of infrared C–O stretching frequencies $\langle\nu_{CO}\rangle$. This average is expected to decrease with increasing π back-bonding. Another quantity useful in this correlation is the sum n_v (the number of valence electrons in the free metal atom) and n_{CO} (the number of CO ligands and their equivalent per metal atom in the compound). It was assumed that the following ligands are equivalent as π acceptors to the indicated number of CO groups: C_7H_7, 2; C_5H_5, C_6H_6, η^4-C_7H_8, $SiCl_3$, $CH_3(CH_3O)C$, CH_3CO, 0.5. Intuitively, n_v changes in a similar manner as effective nuclear charge on the metal atom and is expected to be inversely related to $d\pi$ donor ability of the atom. The quantity n_{CO} measures competition among ligands for $d\pi$ electron density and is also inversely related to the $d\pi$ donor ability of the metal atom in the compound. Therefore, $n_v + n_{CO}$ should decrease with increasing π back-bonding. Table III shows the close correlation of O $1s_{1/2}$, $\langle\nu_{CO}\rangle$, and $n_v + n_{CO}$ for previous data on binary metal carbonyls. The data from this table and the preceding infrared argument are drawn from ref 45, and references to the data in the top section may be found in that article.

As a parallel, we list the multiplicity weighted average $\langle\nu_{CO}\rangle$ vs. O $1s_{1/2}$ binding energy for the clusters studied. The sum $n_v + n_{CO}$ was determined by using for $[Fe_xC(CO)_y]^{n-}$ $8(Fe\text{-}d^8) + y(CO)/x(Fe) + 4(C)/x(Fe) + n/x(Fe)$. Ligands like CH were assigned an unused valency of three and divided by the number of iron atoms. As can be readily seen, there is a good decreasing trend established for $\langle\nu_{CO}\rangle$ based on $n_v + n_{CO}$. Only Fe_4^{2-} is out of the series, suggesting perhaps a unique kind of relatively electron-rich carbide. A correlation exists between

Table III. Correlation of O $1s_{1/2}$ Binding Energies of Carbonyl Complexes and Carbido Clusters with Back-Bonding

compd	O $1s_{1/2}$ binding energy, eV	$\langle\nu_{CO}\rangle$, cm^{-1}	$n_v + n_{CO}$
$[Cr(C_6H_6)(CO)_3]$	538.23	1938	10
$[V(C_7H_7)(CO)_3]$	538.6	1935	10
$[V(C_5H_5)(CO)_4]$	538.7	1963	10
$[Mo(C_5H_5)CH_3(CO)_3]$	538.8	1971	10
$[Mn(C_5H_5)(CO)_3]$	538.85	1974	11
$[Mn_2(CO)_{10}]$	538.89	2017	12
$[Fe(C_7H_8)(CO)_3]$	539.09	2004	12
$\{Cr[CH_3(OCH_3)C](CO)_5\}$	539.1	1984	12
$[Fe(C_4H_6)(CO)_3]$	539.29	2005	12
$[W(CO)_6]$	539.52	2017	12
$[Mo(CO)_6]$	539.61	2021	12
$[Re(CH_3)(CO)_5]$	539.64	2033	12
$[Cr(CO)_6]$	539.66	2018	12
$[MnH(CO)_5]$	539.84	2039	12
$[Mn(CH_3)(CO)_5]$	539.87	2032	12
$[V(CO)_5]$	539.9		11
$[Mn(COCH_3)(CO)_5]$	539.92	2038	12.5
$[Fe(CO)_5]$	540.01	2035	13
$[Ni(CO)_4]$	540.11	2066	14
$[Mn(SiCl_3)(CO)_5]$	540.31	2058	13
$[Fe_2(CH_2)(CO)_8]$		2020[a]	12.8
$[Fe_4C(CO)_{13}]$		2034	12.4
$[Fe_6C(CO)_{16}]^{2-}$	532.4	1957	11.33
$[Fe_4C(CO)_{12}]^{2-}$	530.7	1958	12.5
$[Fe_5C(CO)_{14}]^{2-}$	532.0	1960	11.40
$[Fe_4C(CO)_{12}H]^-$	533.0	1975	11.50
$[Fe_4(\mu\text{-CO})(CO)_{12}H]^-$	532.0	1995	11.75
$[Fe_5C(CO)_{15}]$	532.1	2029	11.8
$[Fe_4(CH)(CO)_{12}H]$	532.3	2032	12.0

[a] Run as solution spectra in CH_2Cl_2. $\langle\nu_{CO}\rangle$ was obtained by weighing traces of the IR spectrum for a weighted average.

molecular charge such that $Fe_4(CO)^0 \simeq Fe_4(CH)^0 \simeq Fe_5^0 \simeq Fe_2(CH_2)^0 > Fe_4(\mu\text{-CO})^- \simeq Fe_4^- > Fe_5^{2-} \simeq Fe_4^{2-} \simeq Fe_6^{2-}$. What is also apparent is that no direct correlation exists between O $1s_{1/2}$ binding energies and $\langle\nu_{CO}\rangle$. The conclusion we draw is that metal cluster-carbonyl stretching frequencies are not correlating with O $1s_{1/2}$ binding energies because the polyhedral arrays' ability to back-bond is altered substantially not only by charge (which is somewhat predictable) but also with the changing nature of the polyhedral carbon atom and the latter is the lesser effect for stretching frequencies except in the lowest coordinate carbon atom in the series, Fe_4^{2-}, where excess charge may be localizing on carbon, leading to substantial changes in the charge at oxygen.

ESCA studies of metal carbides emphasize that the energy of the ejected electrons from the surface metals are nearly always close to that of the bulk metal.[50] Core electrons with energies consistent with their origin at carbon show an increase in binding energy as the metal radius decreases as in ascending a triad and as the electronegativity of a metal increases in going from left to right across the transition series. We measured the ESCA spectra of the orthorhombahedral iron carbide cementite (θ-Fe_3C) and found the majority of surface carbon in the region of graphite and where iron carbide bulk carbon would be expected with a smaller portion at higher binding energy, possibly due to surface carbon, near a value that we assign to polyhedral carbon in our model compounds. Band theory predicts little or no ionicity for carbon in bulk carbide but makes no prediction for surface carbon. Our observation of deshielded carbon relative to graphite at the cementite surface suggests possible ionicity in the sense of carbon-to-metal electron charge transfer for surface carbides.

Approaches to bonding in homogeneous discrete metal carbido clusters have utilized approaches based on LCAO molecular orbital theory to predict a molecular orbital scheme.[73-75] The findings of just such a series of calculations

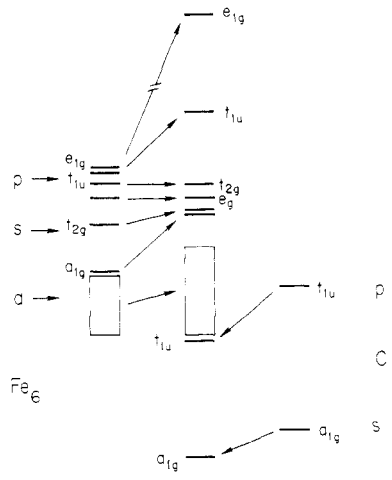

Figure 6. Interaction diagram for the Fe_6C octahedral core.[73]

on hypothetical rhodium clusters emphasize that the larger the cluster the more the molecular orbitals condense into bands.[73] A low-lying metal-derived d-orbital band is primarily responsible for metal–metal polyhedral bonding; s- and p-orbital-derived bands are mainly metal–ligand in nature. In the octahedral carbido clusters exemplified by Fe_6^{2-}, the symmetries of the highest cluster valence molecular orbitals (CVMO) have been calculated to be of t_{1u} and a_{1g} symmetry and carbon s and p orbitals of identical symmetry have the concomitant effect of highly destabilizing the CVMO's of t_{1u} and a_{1g} symmetry as shown in Figure 6. Interstitial carbon, therefore, does not lead to an increase in the number of CVMO's, and it does not change the cluster ligand coordination number preference, but it does stabilize four low-lying CVMO's at the expense of substantially destabilizing four high-lying ligand acceptor orbitals (HLAO). The net effect of this interaction should be observed to lead to higher ν_{CO} stretching frequencies, weaker cluster-carbonyl bonding, and substantial carbido carbon involvement in polyhedral framework bonding. The approach of Wade's rules[38,39] to count carbon atom electrons as framework electrons is therefore justified on this basis. Our observation that the carbido carbon ESCA C $1s_{1/2}$ peak is at a relatively deshielded value suggests electron charge transfer is mainly carbon to metal in the clusters studied.

The effects of sequentially removing metal atoms from the hexagonal close-packed (O_h) array in Fe_6^{2-}, going to a capped square pyramid (C_{4v}) Fe_5^{2-} and then to the folded-butterfly arrangement (C_{2v}) of Fe_4^{2-}, can be approached with use of arguments just advanced. Lowering the carbido carbon coordination number has the effect of reducing symmetry and orbital overlap and lowering the amount of stabilization given t_{1u}- and a_{1g}-derived metal–carbido carbon bonding orbitals and lowering the amount of destabilization imparted to the carbonyl HLAOs. Closer overlap of metal–carbido carbon bonding orbitals with the d-band could lead to enhanced metal–carbido covalency and stabilization of cluster-carbonyl bonding orbitals. Further reduction of the carbido carbon atom would have the tendency to decrease carbon involvement in polyhedral framework orbitals, increase charge at carbon (enhanced nucleophilicity), and further stabilize cluster-carbonyl bonding. This rationale explains the drop and subsequent rise in shielding at iron as displayed by ESCA Fe $2p_{3/2}$ values. This trend appears to be well correlated in the O $1s_{1/2}$ values found for the carbido cluster series Fe_6^{2-}, Fe_5^{2-}, and Fe_4^{2-} as has been mentioned previously.

Acknowledgment. B.A.S. wishes to thank Dow Corp. for a fellowship given 2 years ago for research in this area and The Robert A. Welch Foundation and Research Corp. for support in related areas of research. The ^{57}Fe Mössbauer spectra were obtained with the assistance of Mr. Robert Saxton at Rice University. B.A.S. wishes to express gratitude to his colleague, Dr. Lon J. Wilson, for many helpful criticisms and encouragement. Computer simulation of Mössbauer data was made possible by a grant from the Rice University computer facility, ICSA, administered by Vice President John L. Margrave. The authors also wish to acknowledge the support of R. Hewitt and R. Raymond of Shell Development Co. and Shell for the use of the X-ray photoelectron equipment, which made this study possible. We thank Professor W. N. Delgass (Purdue) and Professor John Eckerdt (University of Texas, Austin) for useful discussions and comments. We thank Dr. John Bradley (Exxon) for a sample of $[Fe_4C(CO)_{13}]$ and Professor Rowland Pettit (University of Texas, Austin) for a sample of $[Fe(CH_2)(CO)_8]$.

(73) Lauher, J. W. *J. Am. Chem. Soc.* **1978**, *100*, 5306.
(74) Lauher, J. W. *J. Am. Chem. Soc.* **1979**, *101*, 2604.
(75) Bernas, H.; Cambell, I. A.; Fruchart, R. *J. Phys. Chem. Solids* **1967**, *28*, 17.
(76) Auger lines may be used to change reference XPS states correcting for relaxation effects. See: Ashe, A. J., III; Bahl, M. K.; Bomben, K. D.; Chan, W. T.; Gimzewski, J. K.; Sitton, P. G.; Thomas, T. D. *J. Am. Chem. Soc.* **1979**, *101*, 1764. This procedure shifts our photolines +1.85 eV, bringing them in line with gas-phase numbers referenced to the Fermi level.

Registry No. $(Et_4N)^+_2[Fe_6C(CO)_{16}]^{2-}$, 11087-55-1; $(Et_4N)^+_2[Fe_5C(CO)_{14}]^{2-}$, 56329-28-3; $Fe_5C(CO)_{15}$, 11087-47-1; $(PPN)^+_2[Fe_4C(CO)_{12}]^{2-}$, 74792-05-5; $(Et_4N)^+[Fe_4C(CO)_{12}H]^-$, 79723-27-6; $Fe_4(CH)(CO)_{12}H$, 74792-06-6; $(C_5H_5N)^+[Fe_4(\mu\text{-}CO)(CO)_{12}H]^-$, 79723-28-7; cementite (Fe_3C), 12011-67-5.